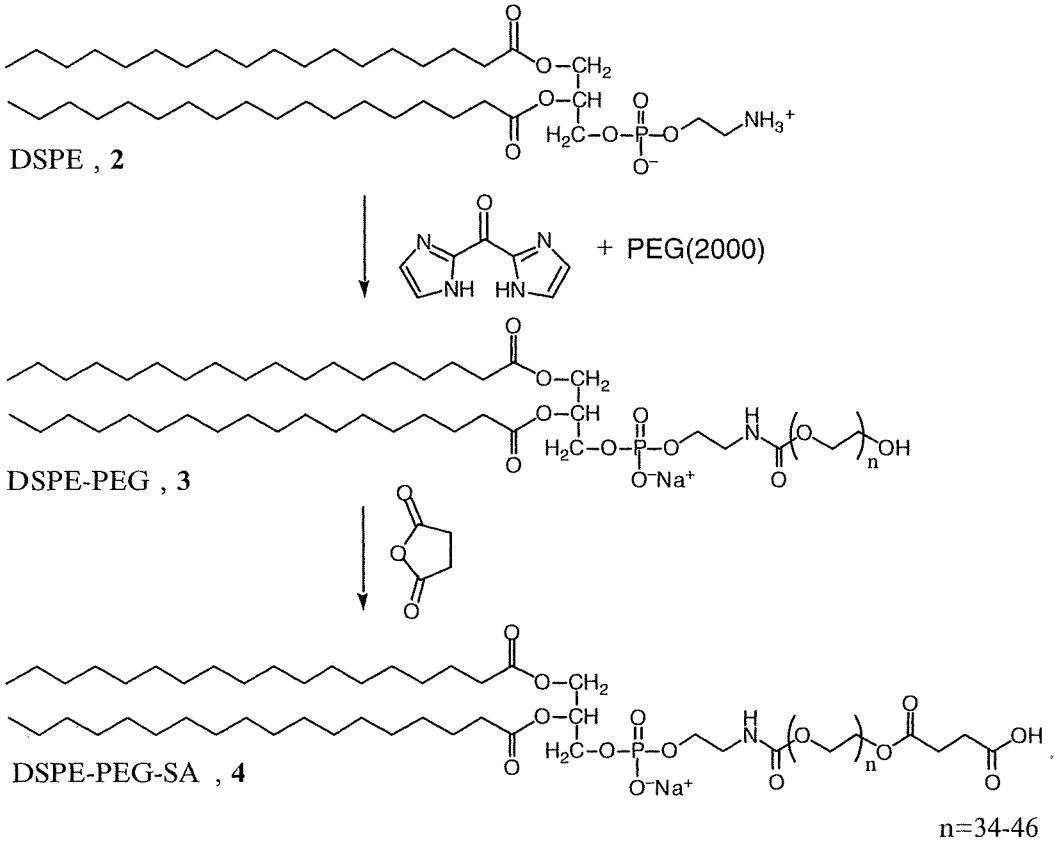

Scheme 1. Pathway for synthesis of DSPE–PEG–SA. Reproduced with permission from (5)

2. To synthesize DSPE–PEG–SA, DSPE (2) 15.0 g and carbonyl diimidazole (CDI) 3.9 g were dissolved in 70 mL of toluene. Reaction was performed at 100 °C for 1 h after addition of triethyl amine 2.0 g. Then, PEG (average molecular weight; 2,000) 40.0 g dissolved in toluene was added dropwise to the solution. The solvent was evaporated in vacuo followed by the reaction, and the product was dissolved in acetone 500 mL and insoluble materials were filtrated and the solvent was evaporated. The reaction mixture was exchanged into Na^+ salt with ion exchange resin. Purification by column chromatography on silica gave 11.4 g of the desired product (3) in a 26% yield. In order to use the PEG-end of obtained DSPE–PEG as a carboxylic group (referred to as (4)); it was allowed to react with succinic anhydride 2.1 g in the presence of pyridine 1.7 g in 100 mL of toluene. After powdering with ether, the yield of 4 was 80%.
3. Preparation of APRPG peptide moiety was carried out by the liquid-phase method as shown in Scheme 2. *N,N'*-dicyclohexylcarbodiimide (DCC, 1.1 equiv. based on peptide) and 1-hydroxybenzotriazol (HOBt, 1.1 equiv. based on peptide)

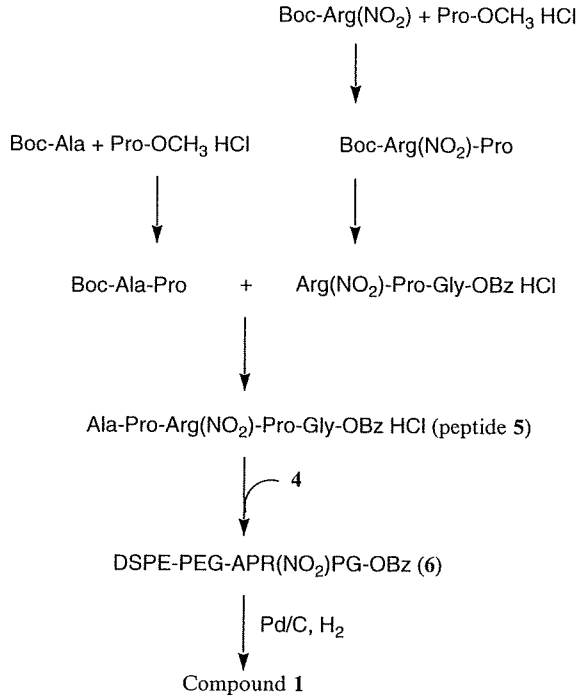

Scheme 2. Pathway for synthesis of DSPE–PEG–APRPG. Reproduced with permission from (5)

were used for peptide coupling in DMF. HCl in 1,4-dioxane was used for deprotection of the Boc group of N-terminal and NaOH was used for deprotection of methyl ester group of C-terminal in water and methanol. In order to avoid racemization, segment condensation was proceeded between Boc-Ala-Pro and Arg(NO_2)-Pro-Gly-OBz to yield 78% of Boc-Ala-Pro-Arg(NO_2)-Pro-Gly-OBz. Next, the Boc protecting group was deprotected by HCl in 1,4-dioxane to obtain peptide (5).

4. Peptide (5) was condensed with (4) (0.93 equiv. based on (5)) in $CHCl_3$ by DCC (1 equiv. based on (5)) and HOBt (1 equiv. based on (5)). The progress of the reaction was monitored by TLC. The reaction was almost complete overnight without any serious side reactions. It was purified by column chromatography on silica. The yield was 83% based on (4). Deprotections of NO_2 group of arginine side chain and benzyl ester group of glycine C-terminal were carried out by 10% palladium–carbon catalytic reduction under hydrogen atmosphere in methanol. It was purified by column chromatography on silica and ion exchange resin. This compound of single spot on TLC was in a 43% yield. This compound (DSPE–PEG–APRPG (1)) was positive for Sakaguchi reagent, while negative for UV lamp on TLC. These showed that NO_2 protecting group and benzyl ester protecting group were deprotected simultaneously (Fig. 1).

3.4. Preparation of PEGylated Liposomal Oligopeptides

1. DSPC and cholesterol with DSPE–PEG or DSPE-PEG–APRPG (10:5:1 as a molar ratio; PEG-lip or APRPG–PEG-lip, respectively) were dissolved in chloroform or chloroform/methanol, dried under reduced pressure, and stored in vacuo for at least 1 h. Liposomes were prepared by hydration of the thin lipid film with 0.3 M glucose, and frozen and thawed for three cycles using liquid nitrogen. Then liposomes were sized by extruding three times through a polycarbonate membrane filter with 100-nm pores (Nucleopore, Maidstone, UK).
2. For an observation of intratumor distribution of liposomes, DiI C18 of the quantity equivalent to 1 mol% of DSPC was added to the liposome. DiI C18-labeled PEG-lip and PEG–APRPG-lip were composed of DSPC, cholesterol, DSPE–PEG and DSPE–PEG–APRPG and DiI C18 (10:5:1:0.1 as molar ratio).
3. For therapeutic experiment, adriamycin (ADM)-encapsulated liposomes were prepared by modification of the remote-loading method as described previously (22). The concentration of ADM was determined by 484 nm absorbance.
4. Particle size and ζ-potential of liposomes diluted with PBS were measured by the use of a Zetasizer Nano ZS (MALVERN, Worcestershire UK, USA).

3.5. Intratumoral Distribution of Liposomal Oligopeptides

DiI C18-labeled liposomes were administered via tail vein of orthotopic tumor model mice (7) on the day 3, 9 and 18 after tumor implantation. Two hours after injection of liposomes, mice were sacrificed and the tumor was dissected. Then, these sections were fluorescently observed by using a microscopic LSM system (Carl Zeiss, Co., Ltd.) (Fig. 2).

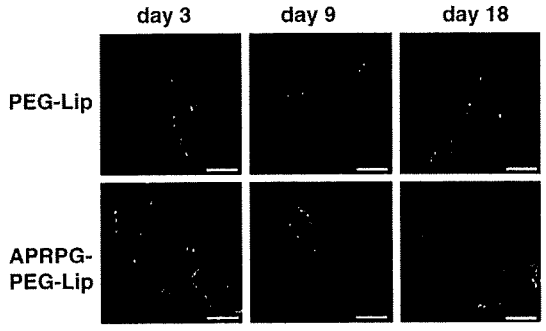

Fig. 2. Intratumoral distribution of DilC18-labeled liposomes in the orthotopic pancreatic tumors. Mice with orthotopic pancreatic tumor were injected with PEG-Lip or APRPG-PEG-Lip labeled with DiI C18 via a tail vein at the day 3, 9, and 18 after tumor implantation. At 2 h after injection of fluorescence-labeled liposomes, frozen-sections of each tumor were prepared. Green portions indicate CD31-positive regions, red portions liposomal distribution, and yellow portions show the localization of liposomes at the site of vascular endothelial cells. Scale bar represents 100 μm. Reproduced with permission from (7)

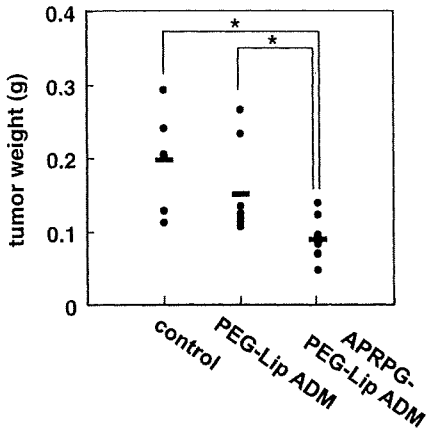

Fig. 3. Therapeutic effect of APRPG–PEG-modified liposome encapsulating ADM on mice with orthotopic pancreatic tumor. Mice with orthotopic pancreatic tumor were injected i.v. with 0.3 M Glucose (control), PEG–LipADM or APRPG–PEG–LipADM for four times at the day 3, 6, 9 and 12 after tumor implantation (n=6–8). Injected dose of liposomal ADM were adjusted to 10 mg/kg as ADM dose in each time. The weight of the tumors was measured at the day 15. Significant differences are shown with asterisks: *P<0.05. Reproduced with permission from (7)

3.6. Therapeutic Efficacy of Adriamycin Encapsulated in Liposomal Oligopeptides

Liposomes encapsulating ADM or 0.3 M glucose solution were administered intravenously into SUIT-2-bearing mice at day 3, 6, 9 and 12 after the implantation of tumor cells. The injected dose of ADM in each administration was 10 mg/kg. The weight of tumor was observed at day 15 (Fig. 3).

3.7. Preparation of DPP–CNDAC Liposomes Modified with Oligopeptides

1. Synthesis of CNDAC and DPP–CNDAC was performed as described previously (16, 17). Briefly, a phosphatidyl group was introduced into CNDAC through transphosphatidylation from 1,2-dipalmitoyl-3-sn-glycerophosphocholine by using phospholipase D.
2. Liposomes were prepared as follows: DPP–CNDAC, DSPC, cholesterol with DSPE–PEG (LipCNDAC/PEG) or DSPE–PEG–APRPG (LipCNDAC/APRPG–PEG) (10/10/5/2 as a molar ratio), or DPP–CNDAC, DSPC, cholesterol without PEG-conjugate (LipCNDAC, 10: 10: 5 as a molar ratio) were dissolved in chloroform/methanol, dried under reduced pressure, and stored in vacuo for at least 1 h. Liposomes were produced by hydration of a thin lipid film with 10 mM phosphate-buffered 0.3 M sucrose (pH 6.8), and frozen and thawed for three cycles by use of liquid nitrogen. Then the liposomes were sized by extrusion thrice through polycarbonate membrane filters with 100-nm-diameter pores. The liposomal solutions were centrifuged at 180,000 × g for 20 min (CS120EX, Hitachi, Japan) to remove the untrapped DPP–CNDAC if present. Then, the liposomes were resuspended in 10 mM phosphate-buffered 0.3 M sucrose.

3. For the determination of the efficacy of trapping DPP–CNDAC in the liposomes, an aliquot of the liposomal solution was solubilized by the addition of reduced Triton X-100, and the amount of DPP–CNDAC was optically determined at 280 nm after the pH of the solution had been adjusted to 1.0. As a result, the encapuslation percent was almost 100%.

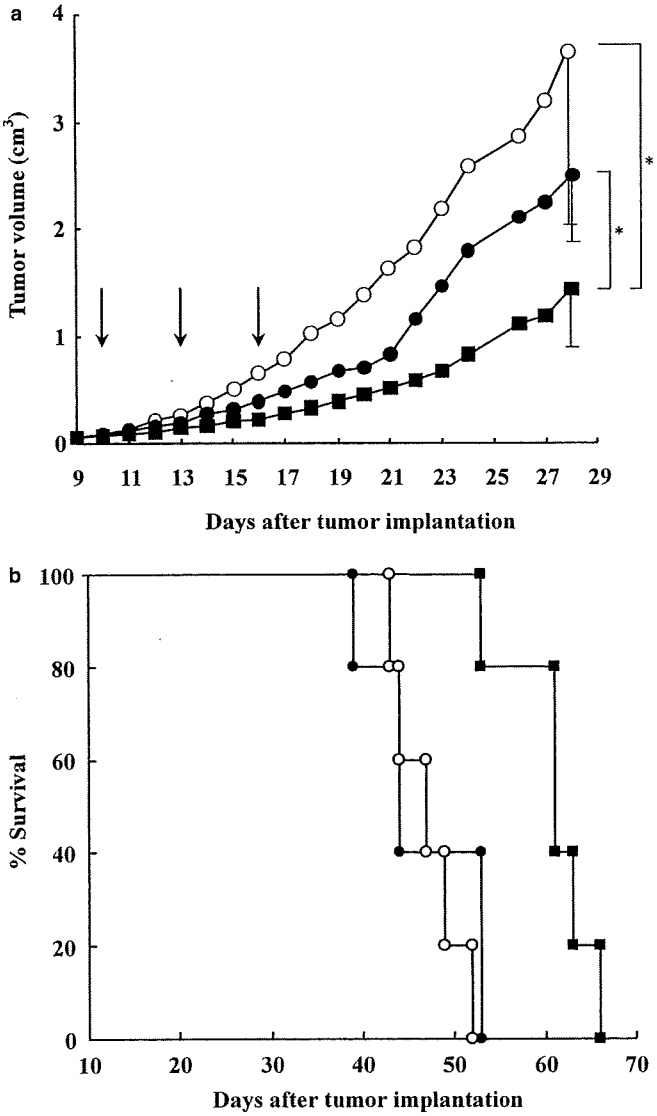

Fig. 4. Therapeutic efficacy of LipCNDAC/APRPG–PEG in tumor-bearing mice. Five-week-old Balb/c male mice (5 or 6 per group) were implanted s.c. with Colon 26 NL-17 carcinoma cells into their left posterior flank. They were injected i.v. with control liposomes (open circle), LipCNDAC/PEG (closed circle) or LipCNDAC/APRPG–PEG (*closed square*) at 15 mg/kg as CNDAC on days 10, 13, and 16 (*arrows*) after tumor implantation. The tumor volume (**a**) and survival time of mice (**b**) were monitored to evaluate the therapeutic efficacy of DPP–CNDAC liposomes. Significant differences from the control liposome-treated group are indicated (*$P<0.05$). Reproduced with permission from (18)

4. For the therapeutic study, control liposomes composed of DPPC, DSPC, and cholesterol (10/10/5 as a molar ratio) were prepared similarly as for the other liposomes.
5. Particle size and ζ-potential of liposomes diluted with PBS were measured by use of a Zetasizer Nano ZS. They were 121 ± 4 nm and −29.2 mV for LipCNDAC, 122 ± 6 nm and −6.1 mv for LipCNDAC/PEG, and 102 ± 2 nm and −3.6 mV for LipCNDAC/APRPG–PEG, respectively.

3.8. Therapeutic experiment with APRPG–PEG-Modified Liposomal DPP–CNDAC

LipCNDAC/PEG, LipCNDAC/APRPG–PEG or control liposomes were administered intravenously into colon 26 NL-17 tumor-bearing mice. The injected dose for each administration was 15 mg/kg as CNDAC moiety. The treatment was started when the tumor volume became approxiamtely 0.1 cm^3. The size of the tumor and the body weight of each mouse were monitored daily thereafter (Fig. 4a). Two bisecting diameters of each tumor were measured with slide calipers to determine the tumor volume. Calculation of the tumor volume was performed by using the formula 0.4 ($a \times b^2$), where "a" is the largest and "b" is the smallest diameter. The calculated tumor volume correlated well with the actual tumor weight ($r = 0.980$) (22). The life spans of tumor-bearing mice were also monitored (Fig. 4b).

4. Notes

1. In general, encapsulation efficiency of drugs into liposomes is dependent on the logP value (octanol/water partition coefficient) of them, when they cannot be liposomalized by special techniques such as a remote-loading method (22). In many cases, it is difficult to encapsulate drugs into liposomes with high encapsulation efficiency since logP value of drugs is not always suit for liposomalization. In addition, it is also difficult to guarantee the quality and the stability of liposomal drugs in such difficult cases. CNDAC is also difficult to be liposomalized with high encapsulation efficiency by a general hydration method. Therefore, phospholipid derivatization of certain drugs to suit liposomal formulations is the useful methodology to develop liposomal drugs.
2. PEG-shielding of the liposomal surface should be useful for designing active targeting DDS with oligopeptides as well as passive targeting. An important aspect of PEGylation is that it serves for not only RES-avoiding but also for the construction of a practical liposomal oligopeptides. In fact, the biodistribution of APRPG-modified DPP–CNDAC liposomes without

PEG was strongly affected by the presence of cyano group of DPP–CNDAC on the liposomal surface. It induced aggregation of the liposomes, resulting in reduced blood circulation of the liposomes. However, the fixed aqueous layer formed by PEG can mask the undesirable surface properties of liposomes, which prevent attenuation of the effect of oligopeptides. The technology used in this study is also applicable to liposomalization of other compounds, DNA or siRNA etc.

3. We indentified oligopeptides specifically bound to tumor angiogenic vessels from a phage-displayed peptide library and applied to a liposomal DDS. The advantage of *in vivo* biopanning the library is that the selected phages have the ability to bind only to angiogenic vessels, not to other tissues. In fact, the amino acid sequences of the phage clones thus obtained were different from any reported sequences. The selected phage clones had high affinity to murine angiogenic vessels.
4. One of the important things to develop liposomal oligopeptides for clinical use, we should investigate whether the peptides selected in the murine model have affinity for angiogenic endothelium in human tumors. In our studies, we demonstrated that our peptides have affinity for human angiogenic endothelium by histochemical staining of the peptides in human cancer samples (2).

Acknowledgements

The authors thank Dr. Noriyuki Maeda and Dr. Yukihiro Namba for the collaboration in the synthesis of APRPG–PEG–DSPE, Dr. Koichi Ogino and Dr. Takao Taki for the phage library project, and Dr. Satoshi Shuto for the synthesis of DPP–CNDAC.

References

1. Asai T, Oku N (2005) Liposomalized oligopeptides in cancer therapy. Methods Enzymol 391:163–176
2. Oku N, Asai T, Watanabe K, Kuromi K, Nagatsuka M, Kurohane K, Kikkawa H, Ogino K, Tanaka M, Ishikawa D, Tsukada H, Momose M, Nakayama J, Taki T (2002) Anti-neovascular therapy using novel peptides homing to angiogenic vessels. Oncogene 21:2662–2669
3. Kondo M, Asai T, Katanasaka Y, Sadzuka Y, Tsukada H, Ogino K, Taki T, Baba K, Oku N (2004) Anti-neovascular therapy by liposomal drug targeted to membrane type-1 matrix metalloproteinase. Int J Cancer 108:301–306
4. Akita N, Maruta F, Seymour LW, Kerr DJ, Parker AL, Asai T, Oku N, Nakayama J, Miyagawa S (2006) Identification of oligopeptides binding to peritoneal tumors of gastric cancer. Cancer Sci 97:1075–1081
5. Maeda N, Takeuchi Y, Takada M, Namba Y, Oku N (2004) Synthesis of angiogenesis-targeted peptides and hydrophobized polyethylene glycol conjugate. Bioorg Med Chem Lett 14:1015–1017

6. Maeda N, Takeuchi Y, Takada M, Sadzuka Y, Namba Y, Oku N (2004) Anti-neovascular therapy by use of tumor neovasculature-targeted long-circulating liposome. J ControlRelease 100:41–52
7. Yonezawa S, Asai T, Oku N (2007) Effective tumor regression by anti-neovascular therapy in hypovascular orthotopic pancreatic tumor model. J Control Release 118:303–309
8. Klibanov AL, Maruyama K, Torchilin VP, Huang L (1990) Amphipathic polyethyleneglycols effectively prolong the circulation time of liposomes. FEBS Lett 268:235–237
9. Sadzuka Y, Nakade A, Hirama R, Miyagishima A, Nozawa Y, Hirota S, Sonobe T (2002) Effects of mixed polyethyleneglycol modification on fixed aqueous layer thickness and antitumor activity of doxorubicin containing liposome. Int J Pharm 238:171–180
10. St. Croix B, Rago C, Velculescu V, Traverso G, Romans KE, Montgomery E, Lal A, Riggins GJ, Lengauer C, Vogelstein B, Kinzler KW (2000) Genes expressed in human tumor endothelium. Science 289:1197–1202
11. Asai T, Shimizu K, Kondo M, Kuromi K, Watanabe K, Ogino K, Taki T, Shuto S, Matsuda A, Oku N (2002) Anti-neovascular therapy by liposomal DPP-CNDAC targeted to angiogenic vessels. FEBS Lett 520:167–170
12. Shimizu K, Asai T, Fuse C, Sadzuka Y, Sonobe T, Ogino K, Taki T, Tanaka T, Oku N (2005) Applicability of anti-neovascular therapy to drug-resistant tumor: Suppression of drug-resistant P388 tumor growth with neovessel-targeted liposomal adriamycin. Int J Pharm 296:133–141
13. Matsumura Y, Maeda H (1986) A new concept for macromolecular therapeutics in cancer chemotherapy: Mechanism of tumoritropic accumulation of proteins and the antitumor agent SMANCS. Cancer Res. 46:6387–6392
14. Maeda N, Miyazawa S, Shimizu K, Asai T, Yonezawa S, Kitazawa S, Namba Y, Tsukada H, Oku N (2006) Enhancement of anticancer activity in antineovascular therapy is based on the intratumoral distribution of the active targeting carrier for anticancer drugs. Biol Pharm Bull 29:1936–1940
15. Katanasaka Y, Ida T, Asai T, Maeda N, Oku N (2008) Effective delivery of an angiogenesis inhibitor by neovessel-targeted liposomes. Int J Pharm 360:219–224
16. Matsuda A, Nakajima Y, Azuma A, Tanaka M, Sasaki T (1991) Nucleosides and nucleotides. 100. 2′-*C*-cyano-2′-deoxy-1-β-D-arabinofuranosyl-cytosine (CNDAC): design of a potential mechanism-based DNA-strand-breaking antineoplastic nucleoside. J Med Chem 34:2917–2919
17. Shuto S, Awano H, Shimazaki N, Hanaoka K, Matsuda A (1996) Nucleosides and nucleotides.150. Enzymatic synthesis of 5′-phosphatidyl derivatives of 1-(2′-*C*-cyano-2-deoxy-β-D-*arabino*-pentofuranosyl) cytosine (CNDAC) and their notable antitumor effects in mice. Bioorg Med Chem Lett 6:1021–1024
18. Asai T, Miyazawa S, Maeda N, Hatanaka K, Katanasaka Y, Shimizu K, Shuto S, Oku N (2008) Antineovascular therapy with angiogenic vessel-targeted polyethyleneglycol-shielded liposomal DPP–CNDAC. Cancer Sci 99:1029–1033
19. Yonezawa S, Asai T, Oku N (2007) Dorsal air sac model. Angiogenesis assays. Wiley, New York, pp 229–238
20. Pasqualini R, Ruoslahti E (1996) Organ targeting in vivo using phage display peptide libraries. Nature 380:364–366
21. Pasqualini R, Koivunen E, Ruoslahti E (1997) αv integrins as receptors for tumor targeting by circulating ligands. Nat Biotechnol 15:542–546
22. Oku N, Doi K, Namba Y, Okada S (1994) Therapeutic effect of adriamycin encapsulated in long-circulating liposomes on Meth-A-sarcoma-bearing mice. Int J Cancer 58:415–419

DEVELOPMENTAL DYNAMICS 237:247–258, 2008

HB-EGF Decelerates Cell Proliferation Synergistically With TGFα in Perinatal Distal Lung Development

Seigo Minami, Ryo Iwamoto,* and Eisuke Mekada

Heparin-binding epidermal growth factor-like growth factor (HB-EGF) is a member of the EGF family of growth factors that is suggested to be involved in distal lung development. In HB-EGF null ($HB^{del/del}$) newborns, a histopathologic analysis revealed abnormally thick saccular walls occurring from embryonic day 18.5 that reduced the terminal saccular space area. HB-EGF gene deletion resulted in a significant increase in cell proliferation, indicating that HB-EGF suppresses distal lung cell proliferation. Furthermore, an analysis of saccular morphology and proliferation in HB-EGF and transforming growth factor-α (TGFα) double-mutant newborns revealed that HB-EGF and TGFα function synergistically in this suppression. Finally, crosses between $HB^{del/del}$ mice and waved 2 mice, a hypomorphic EGF receptor (EGFR) mutant strain, suggest that HB-EGF and EGFR cooperate in this process. Thus, HB-EGF has a novel suppressive function that contributes to decelerating distal lung cell proliferation synergistically with TGFα through EGFR in perinatal distal lung development. ***Developmental Dynamics 237:247–258, 2008.***

Key words: HB-EGF; TGFα; EGFR; distal lung development

Accepted 4 November 2007

INTRODUCTION

In the mouse embryo, the development of the lung begins with the outpouching of an endodermal budding from the foregut at embryonic day (E) 9–9.5 (E9–E9.5). Mouse lung development comprises six different stages: the organogenesis (E9.5–E12), the pseudoglandular stage (E12–E16.5), the canalicular stage (E16.5–E17.5), the saccular stage (E17.5 to postnatal day 4 [P4]), the alveolization phase (P4–P14), and the phase of microvascular maturation (P14–P21) (Ten Have-Opbroek, 1991; Burri, 1999; Roth-Kleiner et al., 2004). The progression from canalicular to saccular stage is especially important for lung development, as terminal sacs and vascularization develop during the canalicular stage. Subsequently, the number of terminal sacs and vascularization rapidly increases in the saccular stage. In this stage, as interstitial tissue thins, the saccular spaces expand, the capillary network forms, and type I and II epithelial cells differentiate. Therefore, the saccular stage, which prepares the distal lung for subsequent alveolarization and

ABBREVIATIONS **E** embryonic day **P** postnatal day **EGF** epidermal growth factor **EGFR** EGF receptor **HB-EGF** heparin-binding EGF-like growth factor **TGFα** transforming growth factor-α **AR** amphiregulin **EPR** epiregulin **BTC** betacellulin **GAPDH** glyceraldehydes-3-phosphate dehydrogenase **PBS** phosphate-buffered saline **PCR** polymerase chain reaction **RT-PCR** reverse transcription-PCR **TSSA** terminal saccular space area **TUNEL** terminal deoxynucleotidyltransferase-mediated dUTP nick-end labeling **DAB** diaminobenzidine.

Department of Cell Biology, Research Institute for Microbial Diseases, Osaka University, Osaka, Japan
Grant sponsor: the Ministry of Education, Culture, Sports, Science, and Technology; Grant number: 18570176; Grant number: 18370079; Grant sponsor: Takeda Science Foundation.
***Correspondence to: Ryo Iwamoto, Department of Cell Biology, Research Institute for Microbial Diseases, Osaka University, 3-1, Yamadaoka, Suita, Osaka 565-0871, Japan. E-mail: riwamoto@biken.osaka-u.ac.jp**

DOI 10.1002/dvdy.21398
Published online 10 December 2007 in Wiley InterScience (www.interscience.wiley.com).

gas exchange upon parturition, is absolutely critical for normal lung development.

In normal lung development, epidermal growth factor receptor (EGFR) signaling is fundamentally established. EGFR null mice exhibit defective branching morphogenesis and saccular formation as well as immature differentiation of type II epithelial cells. These EGFR null mice die within a few days after birth, most likely due to respiratory failure caused by immature lung development (Miettinen et al., 1995, 1997; Sibilia and Wagner, 1995). Such molecular genetic studies demonstrate that EGFR signaling plays a crucial role during the saccular stage of lung development.

However, EGFR signaling is complex. The EGF-ErbB signaling network includes four related tyrosine kinase receptors, EGFR (ErbB1) and the ErbB receptors (ErbB2–4), and it also includes multiple ligands of the EGF/neuregulin superfamily (Holbro and Hynes, 2004). The EGF family ligands that bind to EGFR include EGF, transforming growth factor-α (TGFα), amphiregulin (AR), epiregulin (EPR), betacellulin (BTC), epigen, and heparin-binding EGF-like growth factor (HB-EGF) (Harris et al., 2003).

HB-EGF binds to and activates both EGFR and ErbB4 (Higashiyama et al., 1991; Elenius et al., 1997). HB-EGF is synthesized as a type I transmembrane protein (proHB-EGF), and as other EGF family ligands (Massague and Pandiella, 1993), proHB-EGF is cleaved at the juxtamembrane domain, resulting in the shedding of soluble HB-EGF (sHB-EGF; Goishi et al., 1995). sHB-EGF is a potent mitogen and chemoattractant for several cell types (Raab and Klagsbrun, 1997), while proHB-EGF acts as a juxtacrine growth factor that signals to adjacent neighboring cells in a nondiffusible manner (Iwamoto and Mekada, 2000).

HB-EGF has been implicated in several physiological and pathological processes (Raab and Klagsbrun, 1997). Importantly, analyses of HB-EGF null mice have shown that HB-EGF is a crucial factor for proper heart development and function (Iwamoto et al., 2003; Jackson et al., 2003; Yamazaki et al., 2003; Iwamoto and Mekada, 2006), eyelid development (Mine et al., 2005), skin wounding healing (Shirakata et al., 2005), and skin hyperplasia (Kimura et al., 2005). Notably, HB-EGF has been suggested to be involved in proper lung development, as HB-EGF null newborns exhibit saccular wall thickening, a decrease in the number of sacculi, and the immature differentiation of type II epithelial cells (Jackson et al., 2003). Still, a detailed understanding of the key mechanisms underlying such lung abnormalities remains unclear.

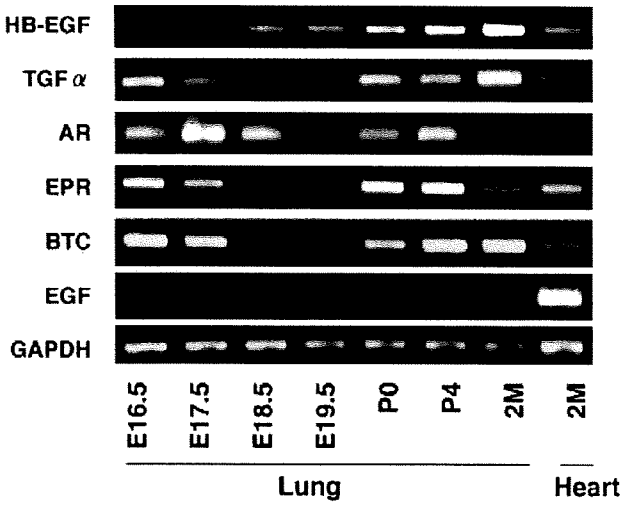

Fig. 1. Chronological analysis of EGFR ligands mRNA expression. RT-PCR of HB-EGF, TGFα, AR, EPR, BTC, EGF, and GAPDH mRNAs from mouse lung at the indicated stages (E16.5–adult) and heart (adult) was performed. For abbreviations, see list.

Therefore, to ascertain how HB-EGF regulates normal lung development, we used HB-EGF null mice to investigate how this specific EGFR ligand regulates cell proliferation in developing pulmonary tissue. Here, we present a novel mechanistic function for HB-EGF in saccular formation. Our data suggest that HB-EGF decelerates cell proliferation synergistically with TGFα selectively through EGFR signaling in perinatal distal lung development.

RESULTS

Postnatal Early Lethality of $HB^{del/del}$ Mice With C57BL/6J Background

We previously reported that approximately half of $HB^{del/del}$ mice with a mixed background (C57BL/6J, ICR, and CBA) show early lethality within a few weeks after birth. The survivors reach adulthood, but many gradually die around 2 to 3 months after birth, probably from heart failure (Iwamoto et al., 2003). In this study, however, we found that the $HB^{del/del}$ mice that have been back-crossed for more than eight generations onto a background of C57BL/6J strain almost all died within a few days after birth and rarely grew up (Fig. S1). No significant difference between $HB^{del/del}$ and $HB^{+/+}$ newborns was noted in body weight ($HB^{del/del}$: 1.42 ± 0.07 g, n = 7 vs. $HB^{+/+}$: 1.38 ± 0.05 g, n = 8; P = 0.67). Although we did not find any abnormalities in our $HB^{del/del}$ lungs with the mixed background of C57BL/6J, ICR and CBA, it has been reported that HB-EGF null mice with the mixed background of C57BL/6J and 129/Sv strains exhibit developmental abnormality in lung (Jackson et al., 2003). We did not detect any obvious histological abnormalities in lung development during pseudoglandular and canalicular stages with the $HB^{del/del}$ mice in C57BL/6J background (data not shown). These observations suggest that any developmental abnormality in lung occurring during the perinatal stage might be a major cause of the perinatal lethality of our $HB^{del/del}$ mice with C57BL/6J background. Therefore, we investigate here the HB-EGF function in lung development, especially focusing on the

perinatal saccular stage, by using $HB^{del/del}$ mice with a C57BL/6J background.

HB-EGF Expression Is Sustained During Prenatal Saccular Stage

First, we performed a chronological analysis of mRNA expression of EGFR ligands including HB-EGF in the lung during canalicular to perinatal saccular stage by reverse transcription-polymerase chain reaction (RT-PCR; Fig. 1). All of the EGFR ligands except EGF have already commenced expression by E16.5. At this stage, however, HB-EGF expression was extremely low when compared with the other EGFR ligands. Expressions of TGFα, AR, EPR, and BTC decreased markedly from E18.5 to E19.5, while only HB-EGF expression was sustained and gradually increased during this stage. Subsequently, expression of all the EGFR ligands except for EGF were increased rapidly just after birth. These chronological expression profiles of EGFR ligands suggest that only HB-EGF is a major factor among EGFR ligands in the developing prenatal lung.

HB-EGF Is Expressed in Lung Alveolar Epithelial Cells

To examine the expression pattern of HB-EGF in lung development, a targeting vector containing the *LacZ* reporter gene for HB-EGF expression was used (Iwamoto et al., 2003). *LacZ*-positive cells were detected in a manner of scattered distributions both in epithelial and interstitial cells of $HB^{del/+}$ and $HB^{del/del}$ newborns and $HB^{del/+}$ adult lungs (Fig. 2). Vascular endothelial cells (as indicated in Fig. 2B) and large bronchial epithelial cells (data not shown) were negative for *LacZ* detection. Although RT-PCR analysis showed HB-EGF expression in lung of the canalicular stage (Fig. 1), we could not detect *LacZ*-positive cells clearly in lung sections of prenatal embryos (data not shown). This disparity might be due to less sensitivity of *LacZ*-staining to that of RT-PCR. The observed pattern of HB-EGF expression in lung suggests that HB-EGF may participate in lung saccular and alveolar development and maintenance of mature lung formation.

Lungs Lacking HB-EGF Exhibit Abnormally Thickened Morphology in Saccular Walls During Saccular Stage

Therefore, to investigate the role of HB-EGF in distal lung development, we examined the morphology of distal lungs in $HB^{del/del}$ embryos and newborns during the saccular stage. $HB^{del/del}$ lungs exhibited an abnormally thickened morphology in saccular walls, an increased number of cells in the saccular septae, and poorly inflated sacculi in parts when compared with wild-type lungs (Fig. 3A). These abnormalities were observed in more than half of the newborn $HB^{del/del}$ lungs. Although $HB^{del/del}$ mice are known to exhibit enlarged cardiac valves and cardiac hypertrophy, these lung phenotypes were obviously not caused by pulmonary edema due to severe heart failure, based on the following observations; first, saccular septae were not edematous histologically. Second, no significant difference between $HB^{del/del}$ and $HB^{+/+}$ lungs were found in wet-to-dry lung weight ratio ($HB^{del/del}$: 5.32 ± 0.23, n = 7 vs. $HB^{+/+}$: 5.63 ± 0.15, n = 8; $P = 0.27$).

To analyze quantitatively these developmental abnormalities in $HB^{del/del}$ lungs, the terminal saccular space areas (TSSA) were measured (Shi et al., 1999; Zhao et al., 2001; Yu et al., 2004). In this analysis, a decrease of TSSA represents an increase of thickness of saccular walls and/or a decrease of saccular inflation. As a result, TSSA was significantly reduced in $HB^{del/del}$ lungs at E18.5, E19.5, and postnatal day (P) 0, but not at E17.5, when compared with those of wild-type lungs at each stage (Fig. 3B). Thus, the abnormalities in $HB^{del/del}$ lung saccular morphology occurred from E18.5 and were remarkable especially at birth (Fig. 3B). These results indicate that HB-EGF is involved in normal distal lung formation during the perinatal saccular stage.

Although it has been reported that the HB-EGF null lung presents an immature differentiation in sacculi (Jackson et al., 2003), our immunohistochemical analysis revealed no remarkable change in the expression of pro-surfactant protein C, a marker for the differentiated type II epithelial cells, between $HB^{+/+}$ and $HB^{del/del}$ lung sacculi (Fig. 4), suggesting that the observed abnormality in lung sacculi of our $HB^{del/del}$ mice is not due to defects in differentiation of saccular epithelium.

HB-EGF Contributes to Deceleration of the Distal Lung Cell Proliferation

Next, we examined whether the thickening of the saccular walls in $HB^{del/del}$ lungs is due to an increased proliferation or to a reduced apoptosis of the distal lung cells. Thus, cell proliferation and apoptosis in distal lungs during perinatal saccular were examined by immunohistochemistry of Ki67, a proliferation marker, and terminal deoxynucleotidyltransferase-mediated dUTP nick-end labeling (TUNEL) staining, respectively.

In distal lungs of E19.5 $HB^{del/del}$ embryos, a significantly increased number of Ki67-positive cells was detected compared with wild-type (Fig. 5A). Consistent with the TSSA analysis (Fig. 3B), in each stage of E18.5 to P0, the ratio of Ki67-positive cells to total cells was significantly increased in $HB^{del/del}$ lung, compared with that of wild-type (Fig. 5B). Moreover, while in the wild-type lung the ratio of Ki67-positive cells had gradually decreased during the perinatal saccular stage, in $HB^{del/del}$ lungs the higher ratio of Ki67-positive cells remained until E19.5 (Fig. 5B). On the other hand, only a few TUNEL-positive cells were detected both in wild-type and $HB^{del/del}$ lungs during this stage, and there was no significant difference in the ratio of TUNEL-positive cells to total cells between wild-type and $HB^{del/del}$ lungs (Fig. 5C,D). These results indicate that abnormally thickened saccular walls in $HB^{del/del}$ lungs is due to increased proliferation, but not to reduced apoptosis, in the distal lung cells and that HB-EGF contributes to the deceleration of such distal lung cell proliferation.

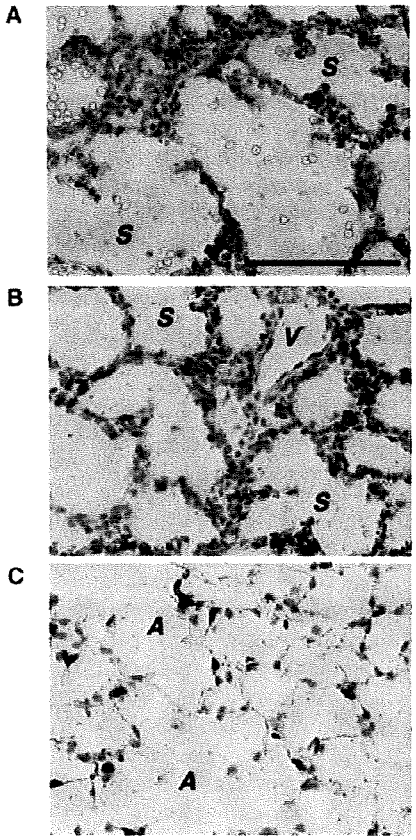

Fig. 2. HB-EGF expression in newborn lung sacculi. *LacZ* staining of (A) $HB^{del/+}$ newborn lung, (B) $HB^{del/del}$ newborn lung, and (C) $HB^{del/+}$ 2-month-old lung. The *LacZ*-stained tissues were counterstained with nuclear fast red. Original magnification: ×400. V, vessel; S, sacculus; A, alveolus. For other abbreviations, see list. Scale bar = 100 μm.

HB-EGF Functions Synergistically With TGFα in Perinatal Distal Lung Development

Recently, we have reported on the synergistic functions of HB-EGF and TGFα in the mouse eyelid closure pro-

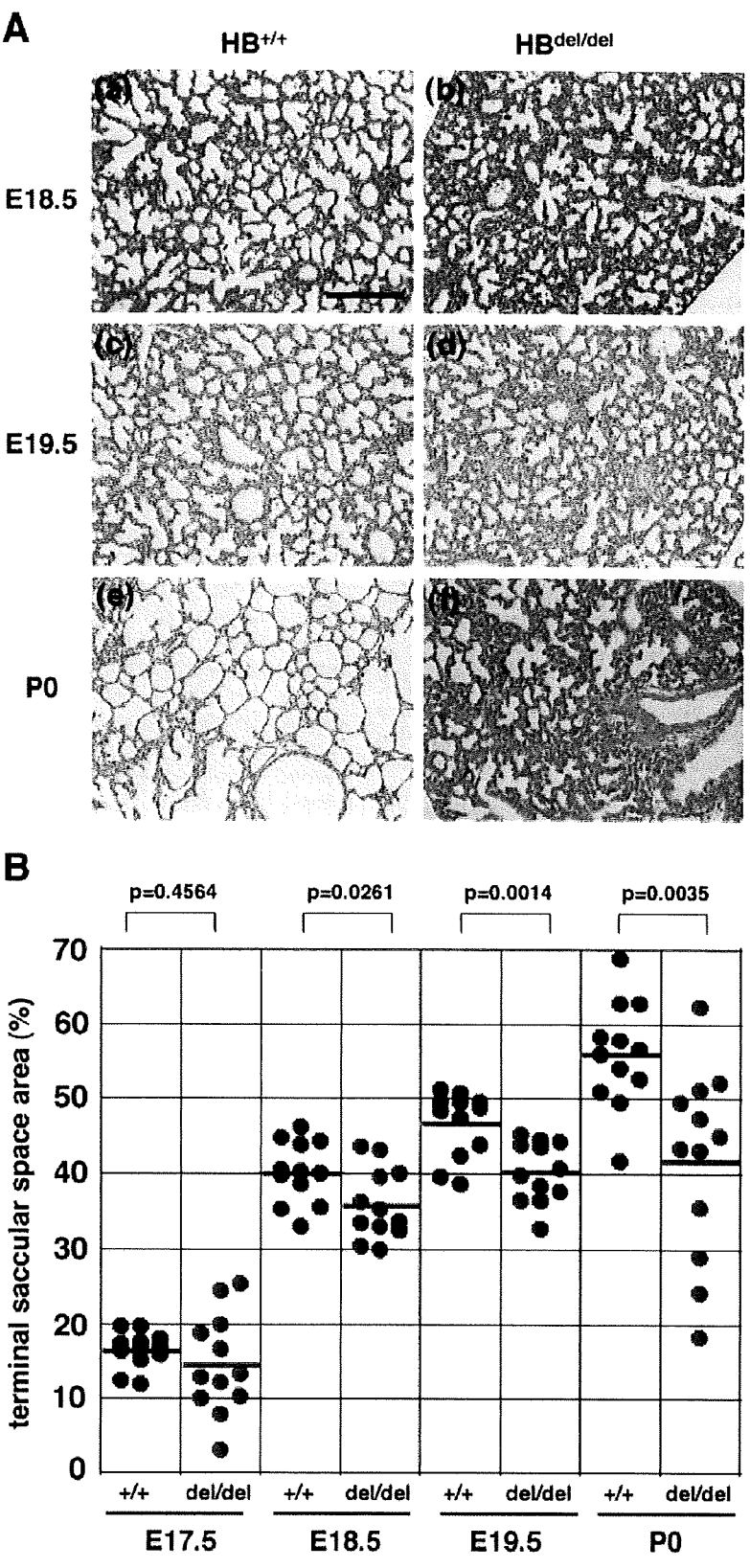

Fig. 3.

Fig. 3. Comparison of embryonic and newborn pup lung morphology between $HB^{del/del}$ and $HB^{+/+}$ genotypes. **A:** Representative hematoxylin/eosin-stained sections of lungs from $HB^{+/+}$(a,c,e) and $HB^{del/del}$ (b,d,f) at E18.5 (a,b), E19.5 (c,d), and newborn (P0) (e,f). **B:**Comparison of TSSA of $HB^{del/del}$ and $HB^{+/+}$ lungs. Each dot represents the percentage of TSSA from a single embryo or a newborn pup, with the horizontal lines representing the mean value for each genotype (n = 12). For abbreviations, see list. Original magnification, ×100. Scale bar = 200 μm in A.

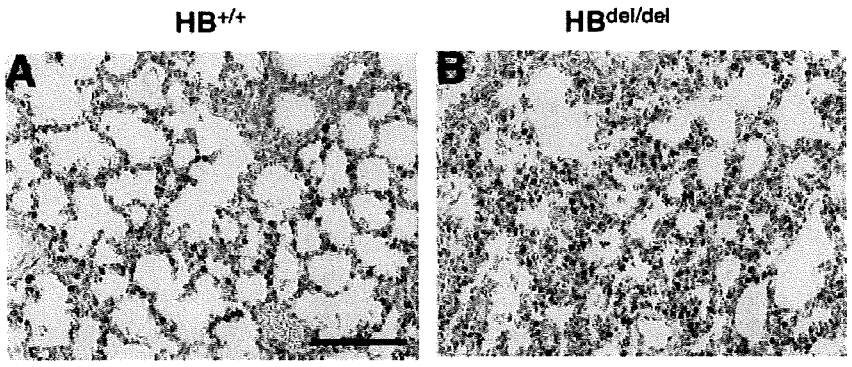

Fig. 4. Immunohistochemistry for pro-surfactant protein C. **A,B:** Sections of $HB^{+/+}$ (A) and $HB^{del/del}$ (B) newborn lung sacculi were immunostained for pro-SpC, a marker for type II epithelial cells. For abbreviations, see list. Original magnification, ×200. Scale bar = 100 μm.

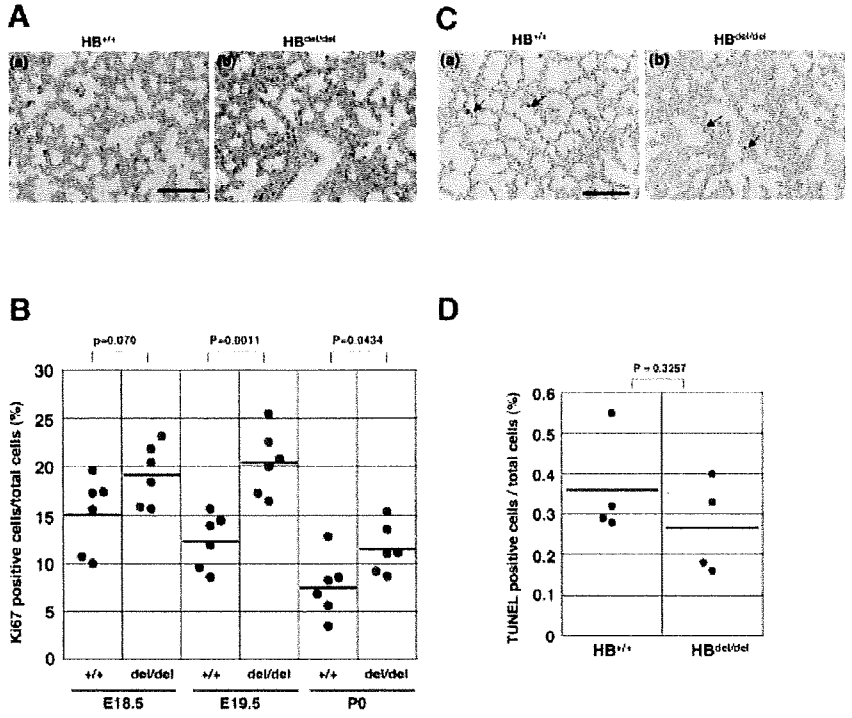

Fig. 5. Comparison of cell proliferation and apoptosis in embryonic and newborn pup lungs from $HB^{del/del}$ and $HB^{+/+}$ genotypes. **A:** Representative sections of $HB^{+/+}$ (a) and $HB^{del/del}$ (b) lungs at E19.5 immunostained for Ki67. **B:** Comparison of percentage of Ki67-positive cells in total lung cells at E18.5, E19.5, and newborn (P0). Each dot represents the percentage of Ki67-positive cells/total cells from a single embryo or a newborn pup, with the horizontal lines representing the mean value for each genotype (n = 6). **C:** Representative TUNEL-stained sections of $HB^{+/+}$ (a) and $HB^{del/del}$ (b) lungs at E19.5. Arrows indicate TUNEL-positive cells. **D:** Comparison of TUNEL-positive cell in lung saccular cells at E19.5. Each dot represents the percentage of TUNEL-positive cells/total cells from a single embryo, with the horizontal lines representing the mean value for each genotype (n = 4). For abbreviations, see list. Original magnification, ×200. Scale bar = 100 μm in A,C.

cess (Mine et al., 2005). Although lung abnormalities have not been reported in TGFα null mice to date, conditional prenatal overexpression of TGFα resulted in abnormal lung morphology at birth (Kramer et al., 2007), suggesting that proper expression of TGFα in lung is important for normal perinatal lung development.

As the expression of TGFα is regulated by HB-EGF in an autocrine manner in keratinocytes (Hashimoto et al., 1994; Piepkorn et al., 1998), we examined whether the defects in lung saccular development in $HB^{del/del}$ lungs were affected by changes in TGFα expression level. Major changes in the level of TGFα expression were not detected between wild-type and $HB^{del/del}$ lungs; however, the level of TGFα might even be somewhat slightly higher in the $HB^{del/del}$ lungs. Likewise, no significant difference was detected in the level of HB-EGF expression between wild-type and $TGF\alpha^{-/-}$ lungs (Fig. S2).

To test for a functional relationship between HB-EGF and TGFα in perinatal lung development, we examined double-null mutants of TGFα and HB-EGF. We tried to breed HB-EGF and TGFα double-null mice; however, intercrosses of $HB^{del/+}$; $Tgf\alpha^{+/-}$ double-heterozygous male and female mice could not produce any $HB^{del/del}$; $Tgf\alpha^{-/-}$ homozygous double-null newborns (in total 260 newborns from 39 litters). Thus, we compared $HB^{del/del}$; $Tgf\alpha^{+/+}$ and $HB^{+/+}$; $Tgf\alpha^{-/-}$ single homozygous null lungs with $HB^{del/del}$; $Tgf\alpha^{+/-}$ and $HB^{del/+}$; $Tgf\alpha^{-/-}$ lungs, respectively, of newborns. First, the TSSA in $Tgf\alpha^{-/-}$ single null lungs was significantly reduced compared with that of wild-type (Fig. 6A,B), indicating that TGFα also contributes to perinatal distal lung development. Then, TSSA was significantly reduced in $HB^{del/del}$; $Tgf\alpha^{+/-}$ lungs compared with $HB^{del/del}$; $Tgf\alpha^{+/+}$ lungs (Fig. 6A,B). On the other hand, TSSA in $HB^{del/+}$; $Tgf\alpha^{-/-}$ lungs was reduced slightly compared with $HB^{+/+}$; $Tgf\alpha^{-/-}$ lungs, without statistical significance. Scattering profiles of TSSA suggest that these differences were due to the increased penetrance, rather than severity, of the TSSA reduction.

Then, regarding proliferation rate of the distal lung cells, the ratio of Ki67-positive cells to the total cells was significantly increased in $HB^{del/del}$; $Tgf\alpha^{+/-}$ and $HB^{del/+}$; $Tgf\alpha^{-/-}$ lungs compared with $HB^{del/del}$; $Tgf\alpha^{+/+}$ and $HB^{+/+}$; $Tgf\alpha^{-/-}$ lungs, respectively. $HB^{+/+}$; $Tgf\alpha^{-/-}$ single null lungs also showed higher ratio of Ki67-positive cells than that of $HB^{+/+}$; $Tgf\alpha^{+/+}$ wild-type lungs, although not statistically significant (Fig. 6C,D).

These results strongly suggest that TGFα also contributes to deceleration of the distal lung cells in a relatively weaker manner than HB-EGF, and

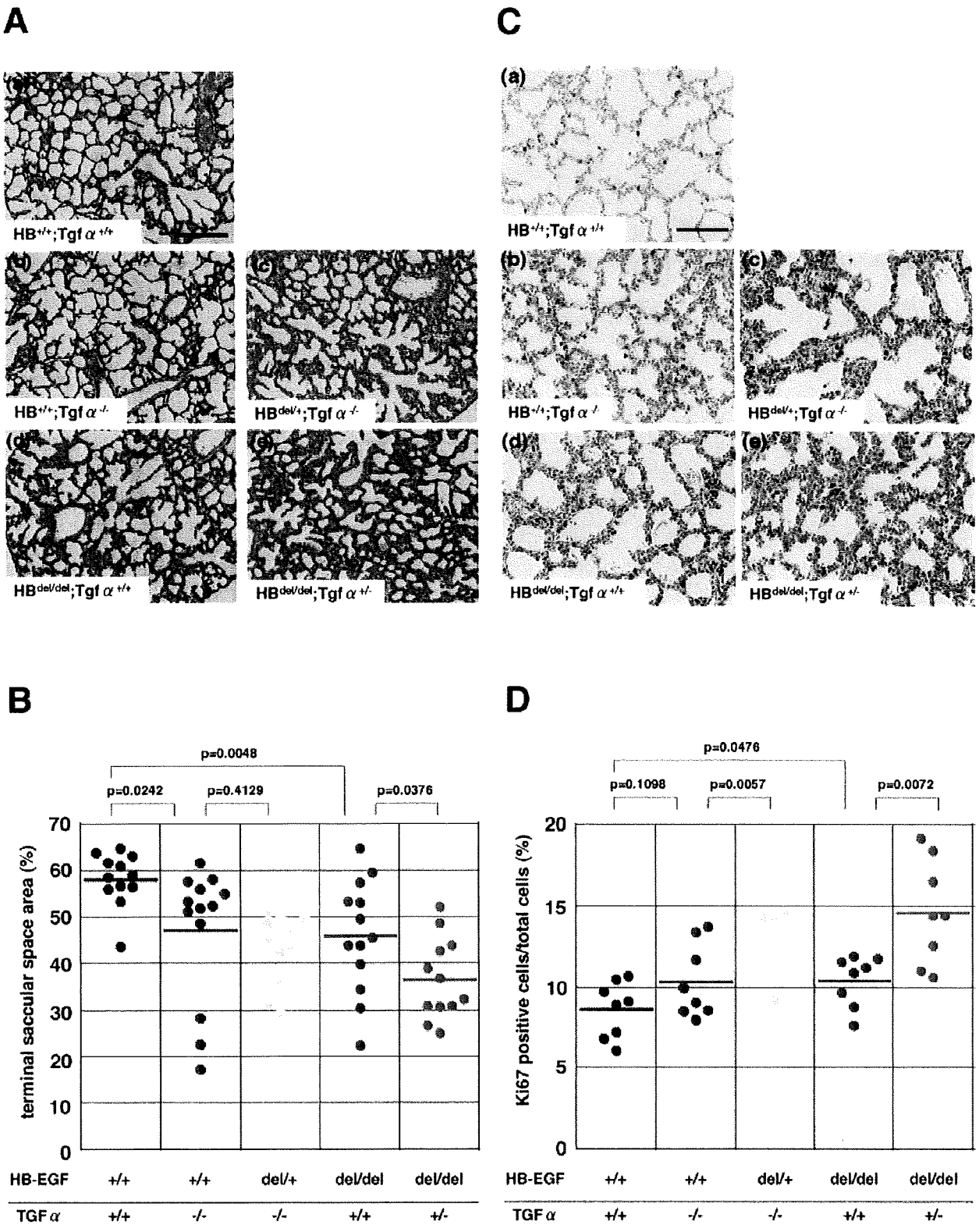
A
C
(a)
(b)
(c)
(d)
(e)
HB+/+;Tgf α +/+
HB+/+;Tgf α -/-
HBdel/+;Tgf α -/-
HBdel/del;Tgf α +/+
HBdel/del;Tgf α +/-
B
D
p=0.0048
p=0.0242
p=0.4129
p=0.0376
p=0.0476
p=0.1098
p=0.0057
p=0.0072
terminal saccular space area (%)
Ki67 positive cells/total cells (%)
HB-EGF +/+ +/+ del/+ del/del del/del
TGF α +/+ -/- -/- +/+ +/-

Fig. 6.

that HB-EGF and TGFα function synergistically in perinatal distal lung formation.

EGFR Is Involved in HB-EGF–Dependent Perinatal Distal Lung Development

EGFR is a receptor for both HB-EGF and TGFα (Harris et al., 2003) and is essential for normal lung development (Miettinen et al., 1995; Sibilia and Wagner, 1995). To determine whether EGFR acts as a receptor for HB-EGF in perinatal distal lung development, we used a hypomorphic EGFR mutant, waved 2, and tested for a genetic interaction with HB-EGF. In waved 2 mice, the kinase activity of EGFR is decreased to less than 10% that of wild-type EGFR, owing to a point mutation in the kinase domain (Luetteke et al., 1994; Fowler et al., 1995). Because intercrosses of $HB^{del/+}$; wa2/+ double-heterozygous male and female mice produced only 3 $HB^{del/del}$; wa2/wa2 double-homozygous newborn (in total 234 newborns from 36 litters), we statistically compared $HB^{del/del}$; wa2/+ and $HB^{del/+}$; wa2/wa2 lungs with $HB^{del/del}$; +/+ and $HB^{+/+}$; wa2/wa2 lungs, respectively, of newborns. Reduction of the TSSA in $HB^{+/+}$; wa2/wa2 single mutant compared with that in wild-type is significantly remarkable. Reduction of TSSA in $HB^{del/del}$; wa2/+ lungs was more frequent than that of $HB^{del/del}$; +/+, although not statistically significant (Fig. 7A,B). We could not detect remarkable differences in the other comparative combinations (Fig. 7A,B).

Regarding proliferation rates, the ratio of Ki67-positive cells to the total cells was significantly increased in $HB^{del/del}$; +/+ and $HB^{+/+}$; wa2/wa2 lungs compared with $HB^{+/+}$; +/+ wild-type lungs. A comparison of the ratio of Ki67-positive cells between $HB^{+/+}$; wa2/wa2 and $HB^{del/+}$; wa2/wa2 lungs showed no significant difference. On the other hand, $HB^{del/del}$; wa2/+ lungs showed a relatively higher ratio of Ki67-positive cells than $HB^{del/del}$; +/+ lungs, although not statistically significant (Fig. 7C,D). Although the statistical significance in this study was lower than those of the case of HB-EGF and TGFα double mutants, these results suggest that EGFR is involved in the inhibitory function of HB-EGF in perinatal distal lung development.

DISCUSSION

We demonstrate here a novel role for HB-EGF in perinatal distal lung development. Our major findings are as follows: (1) HB-EGF is expressed in the lung epithelium and interstitium, and the mRNA level is gradually increased during the canalicular to perinatal saccular stage; (2) HB-EGF contributes to deceleration of perinatal cell proliferation in the distal lung; (3) HB-EGF functions synergistically with TGFα in this stage; (4) EGFR is involved in the HB-EGF function.

Although it has been previously reported that HB-EGF null newborns exhibit abnormal lung morphology (Jackson et al., 2003), the detailed information of such abnormality remains unclear. In this study, we demonstrate using HB-EGF null embryos and newborns that HB-EGF contributes to the deceleration of cell proliferation in the perinatal distal lung, based on the following findings: (1) $HB^{del/del}$ lungs showed significantly lower TSSA scores during perinatal saccular stage after E18.5 as compared to wild-type lungs; (2) in $HB^{del/del}$ lungs, the ratio of Ki67-positive cells in distal lungs was significantly higher than wild-type lungs in each stage examined; (3) only a few apoptotic cells were observed in the lungs in this stage, and no significant difference was detected between wild-type and $HB^{del/del}$ lungs. In this study, the possibility that HB-EGF is also involved in the lung inflation after birth cannot be ruled out; however, the major cause in the abnormally thick saccular walls in HB-EGF null lungs might be due to hypercellularity, because the rate of cell proliferation was significantly increased in the HB-EGF null lungs. Therefore, HB-EGF has an inhibitory function for cell proliferation in distal lungs during perinatal normal lung development. Consequently, the absence of HB-EGF resulted in the persistent deregulated hyperproliferative state in the distal lung cells. It is noteworthy that the ratio of Ki67-positive cells was decreased at birth even in $HB^{del/del}$ lungs, suggesting that there are some other factor(s) compensating HB-EGF functions, as discussed later.

HB-EGF has conventionally been thought of as a growth factor. Indeed, several lines of evidence point to a fundamental role for HB-EGF in cell proliferation and tumorigenesis (Miyamoto et al., 2006). However, no hypoplastic abnormalities have been found in HB-EGF null mice to date; rather, HB-EGF null mice exhibit hyperplastic abnormalities (Iwamoto et al., 2003; Jackson et al., 2003; Yamazaki et al., 2003; Iwamoto and Mekada, 2006) as well as defects in cell migration (Mine et al., 2005; Shirakata et al., 2005). These findings suggest that HB-EGF may not function as a growth factor in developmental and physiological processes. Importantly among these studies, the inhibitory function of HB-EGF for cell proliferation in vivo has also been reported in cardiac valve development (Iwamoto et al., 2003; Jackson et al., 2003; Yamazaki et al., 2003; Iwamoto and Mekada, 2006). In this process, HB-EGF is expressed only in the endocardial cells of developing cardiac valves, mainly during valve remodeling, and causes the inhibition of mesenchymal cell proliferation during valve remodeling. The molecular mechanisms that are involved in the inhibitory function of HB-EGF in both

Fig. 6. Comparison of TSSA and cell proliferation in double mutants of HB-EGF and TGFα newborn pups. **A:** Representative hematoxylin/eosin-stained sections of newborn lungs from $HB^{+/+}$;$Tgf\alpha^{+/+}$ (a), $HB^{+/+}$;$Tgf\alpha^{-/-}$ (b), $HB^{del/+}$;$Tgf\alpha^{-/-}$ (c), $HB^{del/del}$;$Tgf\alpha^{+/+}$ (d), and $HB^{del/del}$;$Tgf\alpha^{+/-}$ (e). **B:** Comparison of TSSA of newborn lungs from $HB^{+/+}$;$Tgf\alpha^{+/+}$, $HB^{+/+}$;$Tgf\alpha^{-/-}$, $HB^{del/+}$;$Tgf\alpha^{-/-}$, $HB^{del/del}$;$Tgf\alpha^{+/+}$, and $HB^{del/del}$;$Tgf\alpha^{+/-}$. Each dot represents the percentage of TSSA from a single newborn pup, with the horizontal lines representing the mean value for each genotype (n = 12). **C:** Representative sections immunostained for Ki67 of newborn (P0) lungs from $HB^{+/+}$;$Tgf\alpha^{+/+}$ (a), $HB^{+/+}$;$Tgf\alpha^{-/-}$ (b), $HB^{del/+}$;$Tgf\alpha^{-/-}$ (c), $HB^{del/del}$;$Tgf\alpha^{+/+}$ (d), and $HB^{del/del}$;$Tgf\alpha^{+/-}$ (e). **D:** Comparison of percentage of Ki67-positive cells in total lung cells of newborn lungs from $HB^{+/+}$;$Tgf\alpha^{+/+}$, $HB^{+/+}$;$Tgf\alpha^{-/-}$, $HB^{del/+}$;$Tgf\alpha^{-/-}$, $HB^{del/del}$;$Tgf\alpha^{+/+}$ and $HB^{del/del}$;$Tgf\alpha^{+/-}$. Each dot represents the percentage of Ki67-positive cells/total cells from a single newborn pup, with the horizontal lines representing the mean value for each genotype (n = 8). For abbreviations, see list. Original magnification, ×200. Scale bar = 100 μm in A,C.

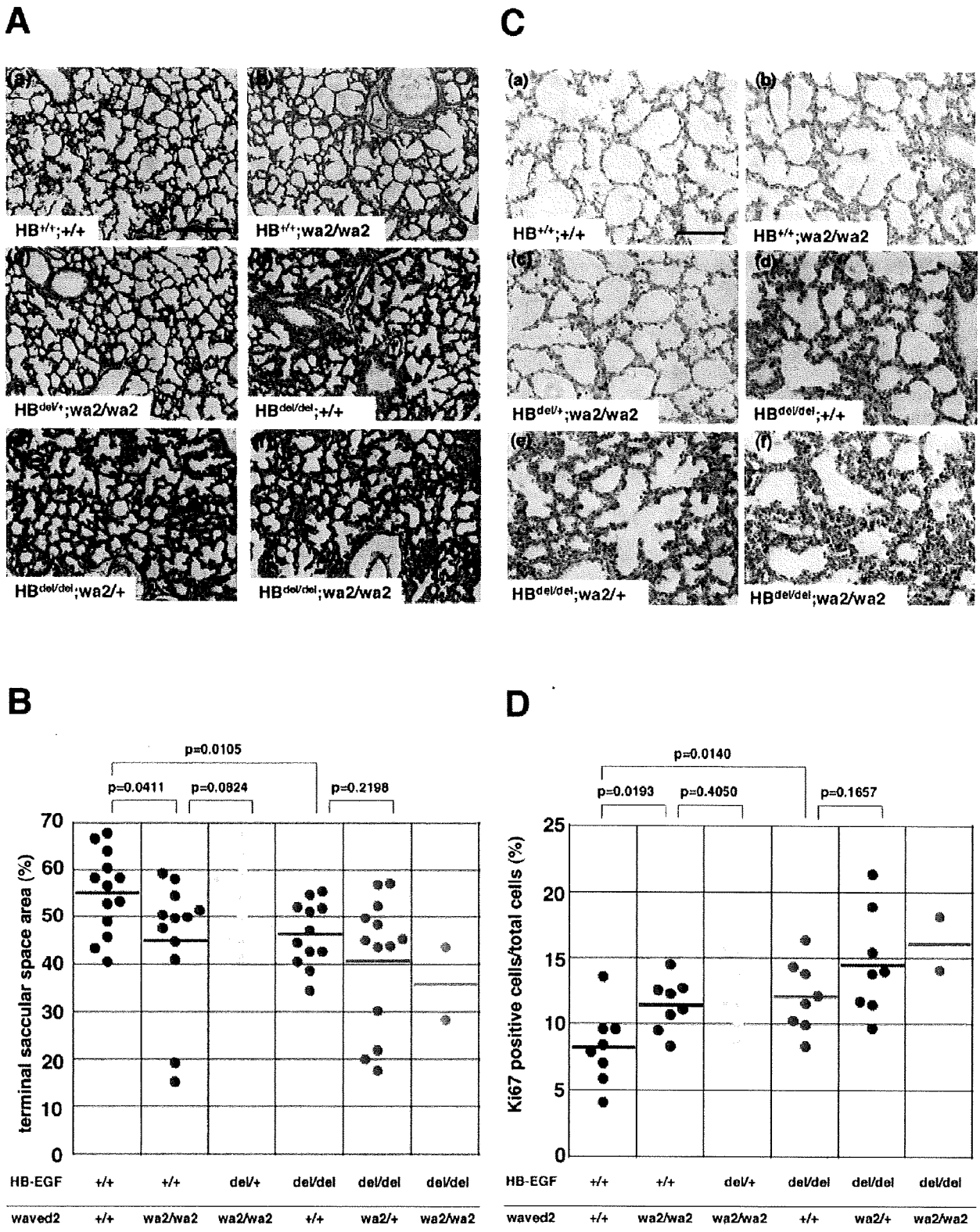
A
C
B
D
HB+/+;+/+
HB+/+;wa2/wa2
HBdel/+;wa2/wa2
HBdel/del;+/+
HBdel/del;wa2/+
HBdel/del;wa2/wa2
p=0.0105
p=0.0411
p=0.0824
p=0.2198
terminal saccular space area (%)
HB-EGF
waved2
p=0.0140
p=0.0193
p=0.4050
p=0.1657
Ki67 positive cells/total cells (%)

Fig. 7.

processes of cardiac valve development and lung saccular development remain unclear. It will be interesting to investigate whether a common mechanism underlies in these two HB-EGF–mediated developmental processes.

A physiological role of TGFα in lung saccular development has remained unknown up to this study. A recent study showed that conditional transgenic mice in which TGFα was overexpressed in prenatal lung had exhibited abnormal lung morphology at birth, characterized by mesenchymal thickening, vascular remodeling, and poor apposition of capillaries to distal airspaces. Moreover, these mice died within a week after birth. In those lungs, proliferation was enhanced and the number of type II epithelial cells was increased (Kramer et al., 2007). By contrast, lung abnormalities have not been reported in TGFα null mice until now. In this study, we show that TGFα has an inhibitory function milder than HB-EGF, and TGFα functions synergistically with HB-EGF in perinatal distal lung development. There was a slight difference in quantitative comparison of TSSA, and there was an insignificant difference in the score of Ki67-positive cells between $TGF\alpha^{+/+}$ and $TGF\alpha^{-/-}$ lungs. Most of the $TGF\alpha^{-/-}$ lungs are morphologically normal, and only a few $TGF\alpha^{-/-}$ lungs exhibited abnormalities characterized by thickened saccular wall and poorly inflated sacculi. However, $HB^{del/del}$; $TGF\alpha^{+/-}$ lungs showed reduced TSSA more frequently and more cell proliferation than $HB^{del/del}$; $TGF\alpha^{+/+}$ lungs with statistical significance. To our knowledge, it is the first evidence that TGFα contributes to normal perinatal lung development. Together with the recent study of the conditional TGFα transgenic mice (Kramer et al., 2007), these results suggest that a delicate regulation of TGFα expression is important for normal lung formation in this stage. Namely, the absence of TGFα induces mild reduction of proliferation as shown in this study, while an excessive expression of TGFα in this stage also results in abnormal saccular morphology caused by hyperproliferation of the saccular cells (Kramer et al., 2007).

TGFα is expressed in bronchioles and saccular epithelia in late gestational lungs (Strandjord et al., 1993, 1994, 1995; Ruocco et al., 1996). It was reported that the expression is decreased by 50% during the transition from the canalicular (E19–E20) to the saccular (E21) stage in late-term fetal rat lung (Kubiak et al., 1992). This change of expression is consistent with our chronological analysis of TGFα mRNA expression by RT-PCR, which revealed that TGFα expression decreases in the prenatal saccular stage and rapidly increases after birth. On the other hand, HB-EGF expression is not down-regulated but rather up-regulated in the prenatal stage. This difference in expression patterns between HB-EGF and TGFα can explain the difference of phenotypic penetrance between $HB^{del/del}$ and $TGF\alpha^{-/-}$ lungs at birth. During prenatal stage, HB-EGF is expressed increasingly and mainly functions in the sacculi, while at birth, both HB-EGF and TGFα are expressed, such that in $TGF\alpha^{-/-}$ lungs, endogenous HB-EGF compensates for the lost function of TGFα during normal perinatal distal lung development.

In perinatal mouse lungs, the expression pattern of other EGFR ligands, including AR, EPR, and BTC, except for EGF, is essentially similar to TGFα. Their expressions are generally once decreased in the prenatal saccular stage. These results also suggest that HB-EGF is the primary factor among EGFR ligands responsible for normal prenatal distal lung development, and that after birth, HB-EGF may regulate cell proliferation synergistically with other EGF family ligands as well as with TGFα. It still remains unclear why the expression of other EGF family ligands except for HB-EGF initially decreases in the prenatal saccular stage during normal lung saccular development. Further study is necessary to clarify the developmental significance of those unique expression profiles and the molecular mechanisms regulating the EGFR ligands in lung saccular development during the saccular stage.

EGFR and ErbB4 are two known cognate receptors for HB-EGF (Higashiyama et al., 1991; Elenius et al., 1997). Loss of EGFR leads to an overall pulmonary malformation, including impaired branching, deficient alveolarization, reduced surfactant protein, and a marked reduction in alveolar volume in the lung (Miettinen et al., 1995; Sibilia and Wagner, 1995; Miettinen et al., 1997). These phenotypes are in part similar to that of HB-EGF null mice. Although ErbB4 null mice die at mid-gestation (E10.5) due to central nervous system and cardiac malformations (Gassmann et al., 1995), ErbB4 null mice genetically rescued from embryonic lethality by heart-specific expression of human ErbB4 are known to reach adulthood. Any lung defects has not been described in these mice (Tidcombe et al., 2003). These studies suggest that EGFR is a possible major receptor for HB-EGF at least in this process.

In this study, we genetically analyze the relationship between HB-EGF and EGFR using waved 2 mice, a hypomorphic EGFR mutant strain. Some $HB^{+/+}$; wa2/wa2 lungs exhibited a reduced TSSA and a significantly higher score in cell proliferation, compared with wild-type lungs. Moreover, $HB^{del/del}$; wa2/+ lungs exhibited a reduced TSSA more frequently and higher score of cell prolif-

Fig. 7. Comparison of TSSA and cell proliferation in double mutants of HB-EGF and waved 2 newborn pups. **A:** Representative hematoxylin/eosin-stained sections of newborn lungs from $HB^{+/+}$;+/+ (a), $HB^{+/+}$;wa2/wa2 (b), $HB^{del/+}$; wa2/wa2 (c), $HB^{del/del}$;+/+ (d), $HB^{del/del}$;wa2/+ (e), and $HB^{del/del}$;wa2/wa2 (f). **B:** Comparison of TSSA of newborn lung alveoli from $HB^{+/+}$;+/+, $HB^{+/+}$;wa2/wa2, $HB^{del/+}$;wa2/wa2, $HB^{del/del}$; +/+, $HB^{del/del}$;wa2/+, and $HB^{del/del}$;wa2/wa2. Each dot represents the percentage of TSSA from a single newborn pup, with the horizontal lines representing the mean value for each genotype (n = 12–13 in $HB^{+/+}$;+/+, $HB^{+/+}$;wa2/wa2, $HB^{del/+}$;wa2/wa2, $HB^{del/del}$;+/+ and $HB^{del/del}$;wa2/+, n = 2 in $HB^{del/del}$;wa2/wa2). **C:** Representative sections immunostained for Ki67 of newborn lung alveoli from $HB^{+/+}$;+/+ (a), $HB^{+/+}$;wa2/wa2 (b), $HB^{del/+}$;wa2/wa2 (c), $HB^{del/del}$;+/+ (d), $HB^{del/del}$;wa2/+ (e), and $HB^{del/del}$;wa2/wa2 (f). **D:** Comparison of percentage of Ki67-positive cells in total lung cells in newborn (P0) lungs from $HB^{+/+}$;+/+, $HB^{+/+}$; wa2/wa2, $HB^{del/+}$;wa2/wa2, $HB^{del/del}$;+/+, $HB^{del/del}$;wa2/+, and $HB^{del/del}$;wa2/wa2. Each dot represents the percentage of Ki67-positive cells/total cells from a single newborn pup, with the horizontal lines representing the mean value for each genotype (n = 8, in $HB^{+/+}$;+/+, $HB^{+/+}$; wa2/wa2, $HB^{del/+}$;wa2/wa2, $HB^{del/del}$;+/+ and $HB^{del/del}$;wa2/+, n = 2 in $HB^{del/del}$;wa2/wa2). For abbreviations, see list. Original magnification, ×200. Scale bar = 100 μm in A,C.

eration than $HB^{del/del}$; +/+ lungs, although without statistical significance. These results suggest that EGFR is involved in HB-EGF–mediated perinatal distal lung development. However, these results do not deny the possibilities that, as well as EGFR, other ErbB family receptors (for example, ErbB4) are also required for normal lung development. The differences in TSSA and proliferation rate between each genotype group of HB-EGF and waved 2 double-mutant mice were much less than the case of HB-EGF and TGFα double-mutant analysis. Furthermore, even waved 2 mice exhibited nearly normal lung morphology at birth and survived. Thus, it will be necessary to study the comprehensive relationship between HB-EGF and ErbB family receptors in lung development.

Almost all HB-EGF null newborns with C57BL/6J backgrounds used in this study died shortly after birth. Impaired development in $HB^{del/del}$ lungs is one possible cause of this early death of the HB-EGF null newborns. However, the penetrance of this lung phenotype is relatively low, and it was observed in only approximately half of $HB^{del/del}$ lungs, whereas the remaining $HB^{del/del}$ lungs were similar to the wild-type morphology. Although it was reported that $HB^{del/del}$ lungs showed immature lung differentiation (Jackson et al., 2003), our immunohistochemical analysis showed no remarkable change in pro-surfactant protein C expression between $HB^{+/+}$ and $HB^{del/del}$ lungs, ruling out the possibility of immature differentiation as a cause of respiratory distress. We unfortunately failed to follow the morphological change in $HB^{del/del}$ lungs after birth because of the severe perinatal lethality of HB-EGF null mice. Thus, it is possible that those lungs of $HB^{del/del}$ with apparently normal morphology rapidly deteriorate after birth, or that we do not notice other hidden severe defects than lungs in HB-EGF null mice. Despite our efforts, it still remains unclear what really causes the early death of HB-EGF null mice.

In conclusion, in the present study, we demonstrated that HB-EGF signaling contributes to perinatal distal lung development. HB-EGF functions synergistically with TGFα, and EGFR signaling regulates the decelerated cell proliferation in the perinatal distal lung. Nonetheless, the complete network of molecular mechanisms regulating these processes remains to be elucidated.

EXPERIMENTAL PROCEDURES

Mice

The generation of HB-EGF null mice ($HB^{del/del}$) has been previously described (Iwamoto et al., 2003). These mice were back-crossed for eight or nine generations onto a background of C57BL/6J strain. TGFα null and waved 2 mice were purchased from Jackson Laboratory. TGFα null mice were maintained on a background of the C57BL/6J strain. Waved 2 mice with a mixed background of C57BL/6JEi and C3H/HeSnJ when purchased, were back-crossed for four or five generations onto a background of C57BL/6J strain. For producing double-mutant mice of TGFα and HB-EGF, or waved 2 and HB-EGF, HB-EGF heterozygous or null mice that were back-crossed for three or four generations onto a background of C57/BL/6J were mated with mice described above. The finding of a vaginal plug was considered as E0.5. Timed pregnant females were killed, and embryos dissected from the uteri were placed in phosphate-buffered saline (PBS). Mice were classified as P0 when birth was witnessed and their breathing activities visualized. All mice used in this investigation were housed in Osaka University Research Institute for Microbial Diseases Animal Care Facility according to the Institutional guidelines for laboratory animals. The use and treatment of animals was approved by the Institutional Biosafety Committee on Biological Experimentation at Osaka University and the Institutional Animal Experimentation Committee at Osaka University.

Reverse Transcription PCR

Total RNA from tissues was isolated using ISOGEN (Invitrogen). One microgram of total RNA was reverse transcribed using a reverse transcriptase, ReverTra Ace (TOYOBO). PCR analysis was performed by using KOD dash (TOYOBO) for HB-EGF (98°C for 10 sec, 60°C for 2 sec, 74°C for 30 sec; 30 cycles), EGF (98°C for 10 sec, 65°C for 2 sec, 74°C for 30 sec; 30 cycles) and glyceraldehydes-3-phosphate dehydrogenase (GAPDH; 98°C for 10 sec, 57°C for 2 sec, 74°C for 30 sec; 30 cycles), and by using KOD plus (TOYOBO) for TGFα (94°C for 15 sec, 68°C for 1 min; 32 cycles), AR (94°C for 15 sec, 68°C for 1 min; 35 cycles), EPR (94°C for 15 sec, 58°C for 30 sec, 68°C for 30 sec; 35 cycles) and BTC (94°C for 15 sec, 60°C for 30 sec, 68°C for 1 min; 33 cycles). The gene-specific primers are as follows: HB-EGF (5′-ATGAAGCTGCTGCCGTCGGT-3′ and 5′-TCAGTGGGAGCTAGCCACGC-3′), TGFα (5′-ATGGTCCCCGCGACCGGACAGCTCGCTCTG-3′ and 5′-ATCTTCAGACCACTGTCTCAGAGTGGCAGC-3′), AR (5′-ATGAGAACTCCGCTGCTACCGCTGGCGCGC-3′ and 5′-CAGCTAGGCAATGGCGTGCACAGTCCCATT-3′), EPR (5′-CAGGCAGTTATCAGCACAAC-3′, and 5′-CCTTGTCCGTAACTTGATGG-3′), BTC (5′-ATGGACCCAACAGCCCCGGGTAGCAGTGTC-3′ and 5′-TAACCGTTAAGCAATATTGGTCTCTTGAAT-3′), EGF (5′-ATGCCCTGGGGCCGAAGGCCAACCTGGCTG-3′ and 5′-TGTAAGCGTGGCTTCCTTCGCCACTGTCCT-3′), and GAPDH (5′-ACCACAGTCCATGCCATCAC-3′, and 5′-TCCACCACCCTGTTGCTGTA-3′). The optimal cycle number for each gene was determined empirically under unsaturating conditions.

LacZ Staining

Dissected newborn lungs were fixed by perfusion of 0.5% glutaraldehyde-2 mM $MgCl_2$ in PBS (pH 7.4) for 1 hr at 4°C before equilibrating in a sucrose solution (30% sucrose-2 mM $MgCl_2$ in PBS, pH 7.4) overnight at 4°C. Sucrose-infused tissues were embedded in OCT compound and then frozen at −80°C. Eight μm sections were fixed again with 4% paraformaldehyde-2 mM $MgCl_2$ in PBS (pH 7.4) for 10 min at 4°C and then stained with X-gal reaction buffer (containing 35 mM potassium ferrocyanide, 35 mM potassium ferricyanide, 2 mM $MgCl_2$, 0.02% Nonidet P-40, 0.01% Na deoxycholate and 1 mg/ml 5-bromo-4-chloro-3-indolyl-β-D-galactoside in PBS, pH7.4) overnight at 37°C. For *LacZ*

staining of adult lungs, procedures of 0.5% glutaraldehyde perfusion and equilibrating in a sucrose solution were omitted. *LacZ*-stained tissues were counterstained with nuclear fast red.

Hematoxylin and Eosin Staining

Newborns were killed by lethal injection of pentobarbital. Thoraces of embryos and newborns were isolated by decapitation and transection at the level of the liver. Skin and soft tissues were removed and then the intact thoraces were immersed in 4% paraformaldehyde in PBS (pH 7.4) at 4°C for 30 hours. After fixation, heart and lung en bloc was carefully isolated from thoracic cavity without punching the lung or diaphragm to minimize any collapse of the lung. The fixed lungs were dehydrated in graded concentration series of ethanol, and embedded in paraffin. Coronal sections were cut at 4 μm thickness and stained with hematoxylin and eosin.

Lung Morphometry

TSSA were measured as previously described (Shi et al., 1999; Zhao et al., 2001; Yu et al., 2004) by using Adobe Photoshop software. Multiple measurements were performed on randomly selected 0.08-mm^2 image fields acquired from two separate sections greater than 50 μm apart from more than 12 fetal or newborn distal lungs of each genotype (Atkinson et al., 2005). Five fields were selected from one section, including two fields from the cranial lobe of the right lung, two fields from the left lung, and one field from the caudal lobe of the right lung. Fields containing large airways and vessels were avoided. The proportion of lung comprising terminal saccular spaces was calculated as percentage of the total examined area of the lung section.

Measurement of Wet-to-Dry Lung Weight Ratio

After body weights were recorded, newborn lungs were removed intact from the thoracic cavity, blotted free of excess fluid, and weighed. Wet lungs were baked for 24 hr at 65°C. Dried lungs were then weighed (Kramer et al., 2007).

Immunohistochemistry and Quantification

Four-μm lung sections were deparaffinized in xylene, followed by rehydration in series of concentrations of ethanol. The endogenous hydrogen peroxidase was quenched with 6% H_2O_2 for 5 min. Sections were incubated with Ki67 rabbit polyclonal antibody (NCL-Ki67p, Novocastra) diluted 1:500 in blocking solution Block Ace (Dainihon Seiyaku) overnight at 4°C, and then incubated with biotinylated goat anti-rabbit secondary antibody (Vector Laboratories) diluted 1:200 for 30 min at room temperature. Staining was developed using a R.T.U. Vectastain kit (Vector Laboratories) and a diaminobenzidine (DAB) substrate (Merck). Sections were counterstained lightly with hematoxylin. Apoptosis was examined by TUNEL according to the manufacturer's protocol (Promega). After immunostaining with Ki67 or TUNEL staining, randomly selected 0.019 or 0.037 mm^2 image fields acquired from two separate sections greater than 50 μm apart from fetal or newborn distal lungs of each genotype (in total, more than 10 fields from 2 sections of each sample), was captured with the Axiocam digital camera and Axiovision software (Zeiss). An average of 3,285 cells per animal (ranging from 1,543 to 6,022 cells per animal) were counted for this analysis. DAB-stained cells were counted as Ki67- or TUNEL-positive on photographs. The proportion of DAB-positive–stained cells per total cell number was represented as the amount of proliferation or apoptosis.

For pro-surfactant C immunohistochemistry, 4-μm lung sections were deparaffinized in xylene, followed by rehydration in series of concentrations of ethanol. The endogenous hydrogen peroxidase was quenched with 3% H_2O_2 in methanol for 15 min. Sections were incubated with rabbit anti-prosurfactant protein-C (proSP-C) antibody (Chemicon) diluted 1:2,000 in blocking solution (4% goat serum and 0.2% TriotnX-100 in PBS) overnight at 4°C, and then incubated with biotinylated goat anti-rabbit secondary antibody (Vector laboratories) diluted 1:200 for 30 min at room temperature. Staining was developed using the aforementioned R.T.U. Vectastain kit and DAB substrate. Sections were counterstained lightly with Hematoxylin.

Data Analysis

Data are presented as means ± SE. Statistical significance was assessed with Student's *t*-test for paired data, or when necessary, the unpaired *t*-test for unequal variances. A value of $P < 0.05$ was considered statistically significant.

ACKNOWLEDGMENTS

We thank M. Hamaoka and T. Kawaguchi for their technical assistance and advice. R.I. and E.M. were funded by grants-in-aid from the Ministry of Education, Culture, Sports, Science, and Technology and E.M. received a grant-in-aid from Takeda Science Foundation.

REFERENCES

Atkinson JJ, Holmbeck K, Yamada S, Birkedal-Hansen H, Parks WC, Senior RM. 2005. Membrane-type 1 matrix metalloproteinase is required for normal alveolar development. Dev Dyn 232:1079–1090.

Burri PH. 1999. Lung development and pulmonary angionenesis. In: Gaultier C, Bourbon J, Post M, editors. Lung disease. New York: Oxford University Press. p 122–151.

Elenius K, Paul S, Allison G, Sun J, Klagsbrun M. 1997. Activation of HER4 by heparin-binding EGF-like growth factor stimulates chemotaxis but not proliferation. EMBO J 16:1268–1278.

Fowler KJ, Walker F, Alexander W, Hibbs ML, Nice EC, Bohmer RM, Mann GB, Thumwood C, Maglitto R, Danks JA, et al. 1995. A mutation in the epidermal growth factor receptor in waved-2 mice has a profound effect on receptor biochemistry that results in impaired lactation. Proc Natl Acad Sci U S A 92:1465–1469.

Gassmann M, Casagranda F, Orioli D, Simon H, Lai C, Klein R, Lemke G. 1995. Aberrant neural and cardiac development in mice lacking the ErbB4 neuregulin receptor. Nature 378:390–394.

Goishi K, Higashiyama S, Klagsbrun M, Nakano N, Umata T, Ishikawa M, Mekada E, Taniguchi N. 1995. Phorbol ester induces the rapid processing of cell surface heparin-binding EGF-like growth factor: conversion from juxta-

crine to paracrine growth factor activity. Mol Biol Cell 6:967–980.
Harris RC, Chung E, Coffey RJ. 2003. EGF receptor ligands. Exp Cell Res 284:2–13.
Hashimoto K, Higashiyama S, Asada H, Hashimura E, Kobayashi T, Sudo K, Nakagawa T, Damm D, Yoshikawa K, Taniguchi N. 1994. Heparin-binding epidermal growth factor-like growth factor is an autocrine growth factor for human keratinocytes. J Biol Chem 269:20060–20066.
Higashiyama S, Abraham JA, Miller J, Fiddes JC, Klagsbrun M. 1991. A heparin-binding growth factor secreted by macrophage-like cells that is related to EGF. Science 251:936–939.
Holbro T, Hynes NE. 2004. ErbB receptors: directing key signaling networks throughout life. Annu Rev Pharmacol Toxicol 44:195–217.
Iwamoto R, Mekada E. 2000. Heparin-binding EGF-like growth factor: a juxtacrine growth factor. Cytokine Growth Factor Rev 11:335–344.
Iwamoto R, Mekada E. 2006. ErbB and HB-EGF signaling in heart development and function. Cell Struct Funct 31:1–14.
Iwamoto R, Yamazaki S, Asakura M, Takashima S, Hasuwa H, Miyado K, Adachi S, Kitakaze M, Hashimoto K, Raab G, Nanba D, Higashiyama S, Hori M, Klagsbrun M, Mekada E. 2003. Heparin-binding EGF-like growth factor and ErbB signaling is essential for heart function. Proc Natl Acad Sci U S A 100: 3221–3226.
Jackson LF, Qiu TH, Sunnarborg SW, Chang A, Zhang C, Patterson C, Lee DC. 2003. Defective valvulogenesis in HB-EGF and TACE-null mice is associated with aberrant BMP signaling. EMBO J 22:2704–2716.
Kimura R, Iwamoto R, Mekada E. 2005. Soluble form of heparin-binding EGF-like growth factor contributes to retinoic acid-induced epidermal hyperplasia. Cell Struct Funct 30:35–42.
Kramer EL, Deutsch GH, Sartor MA, Hardie WD, Ikegami M, Korfhagen TR, Le Cras TD. 2007. Perinatal increases in TGF-{alpha} disrupt the saccular phase of lung morphogenesis and cause remodeling: microarray analysis. Am J Physiol Lung Cell Mol Physiol 293:L314–L27.
Kubiak J, Mitra MM, Steve AR, Hunt JD, Davies P, Pitt BR. 1992. Transforming growth factor-alpha gene expression in late-gestation fetal rat lung. Pediatr Res 31:286–290.
Luetteke NC, Phillips HK, Qiu TH, Copeland NG, Earp HS, Jenkins NA, Lee DC. 1994. The mouse waved-2 phenotype results from a point mutation in the EGF receptor tyrosine kinase. Genes Dev 8: 399–413.
Massague J, Pandiella A. 1993. Membrane-anchored growth factors. Annu Rev Biochem 62:515–541.
Miettinen PJ, Berger JE, Meneses J, Phung Y, Pedersen RA, Werb Z, Derynck R. 1995. Epithelial immaturity and multiorgan failure in mice lacking epidermal growth factor receptor. Nature 376:337–341.
Miettinen PJ, Warburton D, Bu D, Zhao JS, Berger JE, Minoo P, Koivisto T, Allen L, Dobbs L, Werb Z, Derynck R. 1997. Impaired lung branching morphogenesis in the absence of functional EGF receptor. Dev Biol 186:224–236.
Mine N, Iwamoto R, Mekada E. 2005. HB-EGF promotes epithelial cell migration in eyelid development. Development 132: 4317–4326.
Miyamoto S, Yagi H, Yotsumoto F, Kawarabayashi T, Mekada E. 2006. Heparin-binding epidermal growth factor-like growth factor as a novel targeting molecule for cancer therapy. Cancer Sci 97:341–347.
Piepkorn M, Pittelkow MR, Cook PW. 1998. Autocrine regulation of keratinocytes: the emerging role of heparin-binding, epidermal growth factor-related growth factors. J Invest Dermatol 111: 715–721.
Raab G, Klagsbrun M. 1997. Heparin-binding EGF-like growth factor. Biochim Biophys Acta 1333:F179–F199.
Roth-Kleiner M, Hirsch E, Schittny JC. 2004. Fetal lungs of tenascin-C-deficient mice grow well, but branch poorly in organ culture. Am J Respir Cell Mol Biol 30:360–366.
Ruocco S, Lallemand A, Tournier JM, Gaillard D. 1996. Expression and localization of epidermal growth factor, transforming growth factor-alpha, and localization of their common receptor in fetal human lung development. Pediatr Res 39:448–455.
Shi W, Heisterkamp N, Groffen J, Zhao J, Warburton D, Kaartinen V. 1999. TGF-beta3-null mutation does not abrogate fetal lung maturation in vivo by glucocorticoids. Am J Physiol 277:L1205–L1213.
Shirakata Y, Kimura R, Nanba D, Iwamoto R, Tokumaru S, Morimoto C, Yokota K, Nakamura M, Sayama K, Mekada E, Higashiyama S, Hashimoto K. 2005. Heparin-binding EGF-like growth factor accelerates keratinocyte migration and skin wound healing. J Cell Sci 118:2363–2370.
Sibilia M, Wagner EF. 1995. Strain-dependent epithelial defects in mice lacking the EGF receptor. Science 269:234–238.
Strandjord TP, Clark JG, Hodson WA, Schmidt RA, Madtes DK. 1993. Expression of transforming growth factor-alpha in mid-gestation human fetal lung. Am J Respir Cell Mol Biol 8:266–272.
Strandjord TP, Clark JG, Madtes DK. 1994. Expression of TGF-alpha, EGF, and EGF receptor in fetal rat lung. Am J Physiol 267:L384–L389.
Strandjord TP, Clark JG, Guralnick DE, Madtes DK. 1995. Immunolocalization of transforming growth factor-alpha, epidermal growth factor (EGF), and EGF-receptor in normal and injured developing human lung. Pediatr Res 38:851–856.
Ten Have-Opbroek AA. 1991. Lung development in the mouse embryo. Exp Lung Res 17:111–130.
Tidcombe H, Jackson-Fisher A, Mathers K, Stern DF, Gassmann M, Golding JP. 2003. Neural and mammary gland defects in ErbB4 knockout mice genetically rescued from embryonic lethality. Proc Natl Acad Sci U S A 100:8281–8286.
Yamazaki S, Iwamoto R, Saeki K, Asakura M, Takashima S, Yamazaki A, Kimura R, Mizushima H, Moribe H, Higashiyama S, Endoh M, Kaneda Y, Takagi S, Itami S, Takeda N, Yamada G, Mekada E. 2003. Mice with defects in HB-EGF ectodomain shedding show severe developmental abnormalities. J Cell Biol 163: 469–475.
Yu H, Wessels A, Chen J, Phelps AL, Oatis J, Tint GS, Patel SB. 2004. Late gestational lung hypoplasia in a mouse model of the Smith-Lemli-Opitz syndrome. BMC Dev Biol 4:1.
Zhao J, Chen H, Peschon JJ, Shi W, Zhang Y, Frank SJ, Warburton D. 2001. Pulmonary hypoplasia in mice lacking tumor necrosis factor-alpha converting enzyme indicates an indispensable role for cell surface protein shedding during embryonic lung branching morphogenesis. Dev Biol 232:204–218.